Mining Brain Region Connectivity for Alzheimer's Disease Study via Sparse Inverse Covariance Estimation

Liang Sun[1,2], Rinkal Patel[2], Jun Liu[1], Kewei Chen[4], Teresa Wu[3], Jing Li[3], Eric Reiman[4], Jieping Ye[1,2]
[1]Center for Evolutionary Functional Genomics, The Biodesign Institute, Arizona State University, Tempe, AZ 85287
[2]Department of Computer Science and Engineering, Arizona State University, Tempe, AZ 85287
[3]Department of Industrial Engineering, Arizona State University, Tempe, AZ 85287
[4]Banner Alzheimer's Institute and Banner PET Center, Banner Good Samaritan Medical Center, Phoenix, AZ 85006

ABSTRACT

Effective diagnosis of Alzheimer's disease (AD), the most common type of dementia in elderly patients, is of primary importance in biomedical research. Recent studies have demonstrated that AD is closely related to the structure change of the brain network, i.e., the connectivity among different brain regions. The connectivity patterns will provide useful imaging-based biomarkers to distinguish Normal Controls (NC), patients with Mild Cognitive Impairment (MCI), and patients with AD. In this paper, we investigate the sparse inverse covariance estimation technique for identifying the connectivity among different brain regions. In particular, a novel algorithm based on the block coordinate descent approach is proposed for the direct estimation of the inverse covariance matrix. One appealing feature of the proposed algorithm is that it allows the user feedback (e.g., prior domain knowledge) to be incorporated into the estimation process, while the connectivity patterns can be discovered automatically. We apply the proposed algorithm to a collection of FDG-PET images from 232 NC, MCI, and AD subjects. Our experimental results demonstrate that the proposed algorithm is promising in revealing the brain region connectivity differences among these groups.

Categories and Subject Descriptors

H.2.8 [**Database Management**]: Database Applications - Data Mining; J.3 [**Life and Medical Sciences**]: Health, Medical information systems

General Terms

Algorithm

Keywords

Brain network, Alzheimer's disease, neuroimaging, FDG-PET, sparse inverse covariance estimation

KDD'09, June 28–July 1, 2009, Paris, France.

1. INTRODUCTION

Alzheimer's Disease (AD) is a progressively neurodegenerative disease. It is the most common type of dementia in elderly patients. Currently, approximately 5 million people (about 10% of the population over 60) in the U.S. are afflicted by AD. The estimated direct cost to care the patients is over $100 billion per year. As the population ages over the next several decades, the AD cases and the associated costs are expected to go up dramatically. AD researchers have thus intensified their efforts to investigate ways to delay, cure, or prevent the onset and progression of AD.

Objective and quantitative criteria, so called, biomarkers, are essential to evaluate the effectiveness of a potential treatment or prevention strategy. Although clinical assessment and neuropsychological tests provide valuable information for AD diagnosis [19, 11], recent studies have demonstrated that imaging parameters from brain scans are more sensitive and consistent measures of disease progression than cognitive assessment [20]. Some studies have shown that imaging measures correlate with cognitive test performance in Mild Cognitive Impairment (MCI) and AD – an initial step in the validation of markers that accurately predict the course of the disease. Thus, the neuroimaging research offers great potential to identify the sensitive and specific biomarkers that can distinguish between different types of subjects and open up opportunities to implement treatments in the early stages of disease when intervention may be most beneficial.

There are two commonly used neuroimaging techniques for AD study: [18F]-2-fluoro-2-deoxy-D-glucose positron emission tomography (FDG-PET) and volumetric Magnetic Resonance Imaging (MRI). FDG-PET is a functional imaging technique that measures the cerebral metabolic rate for glucose. MRI is a high-resolution structural imaging technique that allows for the visualization of brain anatomy with high degree of contrast between the brain tissues. These imaging techniques have been shown to be effective for AD study [1, 30].

Recent studies have demonstrated that AD is closely related to the alternations of the brain network, i.e., the connectivity among different brain regions [7, 23, 24]. It has been shown that the brain regions are moderately or less inter-connected for AD patients, and cognitive decline in AD patients is associated with disrupted functional connectivity in the brain [24]. The connectivity patterns may be useful as imaging-based biomarkers to distinguish Normal Controls, MCI and AD patients. It is thus important to develop computational tools for identifying the connectivity among different brain regions.

In this paper, we study the **S**parse **I**nverse **C**ovariance **E**stimation (SICE) for the identification of brain region connectivity. SICE originates from the more broad problem of covariance matrix estimation from data [3]. It has been observed that the covariance matrix can be estimated robustly when enough entries of the inverse covariance matrix are set to zero [8]. On the other hand, it has been demonstrated in the literature that many inverse covariance matrices are sparse, such as genetic interaction networks [13, 25]. Furthermore, the sparse inverse covariance can be interpreted from the perspective of the undirected graphical model [16] which models and explains the relationship among a set of variables. In practice, it is usually reasonable to assume that the patterns of some variables can be predicted by a small subset of all variables, which leads to the sparsity of the inverse covariance matrix in the multivariate Gaussian distribution. These observations in theory and practice motivate the wide use of the sparse inverse covariance estimation. It has been shown to be useful in various applications, including evaluating patterns of association among variables [9], exploration of genetic networks [17], senator voting records analysis [2], hyperspectral image classification [4], and speech recognition [5].

In this paper, we propose a novel algorithm for SICE. Unlike most of the existing algorithms [2, 6, 12, 15, 17, 18], the proposed SICE algorithm estimates the inverse covariance matrix directly. One appealing feature of the proposed algorithm is that it allows the user feedback (e.g., prior domain knowledge) to be incorporated into the estimation process by imposing additional constraints in the optimization formulation, while discovering the connectivity patterns automatically. We apply the proposed algorithm to a collection of FDG-PET images from 232 NC, AD, and MCI subjects enrolled in the Alzheimer's Disease Neuroimaging Initiative (ADNI)[1]. The experimental results reveal several interesting connectivity patterns among different brain regions. Our results also demonstrate the benefit of using the user feedback for the understanding of the brain network.

The rest of the paper is organized as follows. Section 2 provides the background on AD and two neuroimaging techniques including MRI and FDG-PET. In section 3, we review the sparse inverse covariance estimation. The proposed algorithm is presented in section 4. Section 5 presents the experimental results. Section 6 concludes the paper and discusses some future work.

2. BACKGROUND

2.1 Alzheimer's Disease and Neuroimaging

Alzheimer's disease is an irreversible, progressive brain disease which slowly destroys memory and thinking skills, eventually even the ability to carry out simple daily tasks [14]. Most AD diagnosis is based on clinical and psychometric assessment. [19] summarizes the clinical criteria for clinically probable AD, which include insidious onset and progressive impairment of memory and other cognitive functions. Mini Mental State Examination (MMSE) is one of a number of cognitive tests carried out to clinical patients for disease diagnosis (MCI, AD, and NC classification) [11]. Although clinical assessment and neuropsychological tests provide valuable information for AD diagnosis, recent studies have demonstrated that imaging parameters from brain scans are more sensitive and consistent measures of disease progression than cognitive assessment [20].

[1]http://www.loni.ucla.edu/ADNI/

Table 1: Test Data Set.

Subjects	No.	Mean-Age	Std deviation-Age
AD-Male	27	76.74	6.75
AD-Female	22	75.59	6.11
MCI-Male	76	75.84	6.12
MCI-Female	40	75.85	6.08
NC-Male	43	76.74	6.26
NC-Female	24	75.33	5.82

Medical Imaging techniques like MRI and FDG-PET have been used widely in understanding the human brain. Volumetric MRI is a high-resolution structural imaging technique that allows for the visualization of brain anatomy with high degree of contrast between the brain tissues. T1-weighting of the MRI procedure is now a routine for visualizing and investigating brain gray, white and cerebrospinal fluid (CSF) tissue. With this procedure, the contrast between these different brain tissue types are high and segmentation of the MRI data to different tissue types becomes feasible. The structural information is used to study the volumetric changes in the brain related AD, which causes significant shrinkages in the gray matter, regionally and globally.

PET is a functional imaging technique that captures the metabolic activity of various brain regions. The PET scanner detects pairs of gamma rays emitted by a positron-emitting radionuclide (tracer), which is introduced into the body on a biologically active molecule. If the biologically active molecule chosen for PET is FDG, an radioactive analogue of glucose, the concentrations of tracer imaged then give tissue metabolic activity, in terms of regional glucose uptake.

2.2 Data Acquisition and Preprocessing

FDG-PET 3D images used in this study were from 49 AD's, 67 NC's, 116 MCI's downloaded from ADNI. All the FDG-PET images available from ADNI undergo various processing like co-registration to a common coordinate system, averaging, standardization of image and voxel size and uniformity in resolution. Demographic information of the subjects is shown in Table 1. Using SPM5[2], the PET images are normalized to the standard Montreal Neurological Institute (MNI) template space, and the normalization quality was visually inspected.

2.3 Regional Averages using AAL

Our current research is based on the regions of interest (ROI) from the PET data. The whole brain volume is divided into 116 anatomical volumes of interest (AVOI), defined by Automated Anatomical Labeling (AAL) [28]. Then the average of the voxel intensities over each AVOI for each subject is extracted and used for our analysis. Neuroimaging AD researchers have identified a number of AD affected brain regions, such as hippocampus, that are a sub-set of the 116 AAL defined ROIs. The domain expertise is useful for understanding the results of future data analysis. Table 2 gives the names of the 116 AVOIs.

[2]http://www.fil.ion.ucl.ac.uk/spm/

Table 2: 116 brain regions defined by AAL. The regions highlighted are those used in our experiments.

Sr.	Name	Sr.	Name	Sr.	Name	Sr.	Name
1	Precentral_L	30	Insula_R	**59**	**Parietal_Sup_L**	**88**	**Tem_Pole_Mid_R**
2	Precentral_R	31	Cingulum_Ant_L	**60**	**Parietal_Sup_R**	**89**	**Temporal_Inf_L**
3	Frontal_Sup_L	32	Cingulum_Ant_R	**61**	**Parietal_Inf_L**	**90**	**Temporal_Inf_R**
4	Frontal_Sup_R	33	Cingulum_Mid_L	**62**	**Parietal_Inf_R**	91	Cerebelm_Crus1_L
5	Frontal_Sup_Orb_L	34	Cingulum_Mid_R	63	SupraMarginal_L	92	Cerebelm_Crus1_R
6	Frontal_Sup_Orb_R	**35**	**Cingulum_Post_L**	64	SupraMarginal_R	93	Cerebelm_Crus2_L
7	Frontal_Mid_L	**36**	**Cingulum_Post_R**	65	Angular_L	94	Cerebelm_Crus2_R
8	Frontal_Mid_R	**37**	**Hippocampus_L**	66	Angular_R	95	Cerebelum_3_L
9	Frontal_Mid_Orb_L	**38**	**Hippocampus_R**	**67**	**Precuneus_L**	96	Cerebelum_3_R
10	Frontal_Mid_Orb_R	**39**	**ParaHippo_L**	**68**	**Precuneus_R**	97	Cerebelum_4_5_L
11	Frontal_Inf_Oper_L	**40**	**ParaHippo_R**	69	Paracentral_Lob_L	98	Cerebelum_4_5_R
12	Frontal_Inf_Oper_R	41	Amygdala_L	70	Paracentral_Lob_R	99	Cerebelum_6_L
13	Frontal_Inf_Tri_L	42	Amygdala_R	71	Caudate_L	100	Cerebelum_6_R
14	Frontal_Inf_Tri_R	43	Calcarine_L	72	Caudate_R	101	Cerebelum_7b_L
15	Frontal_Inf_Orb_L	44	Calcarine_R	73	Putamen_L	102	Cerebelum_7b_R
16	Frontal_Inf_Orb_R	45	Cuneus_L	74	Putamen_R	103	Cerebelum_8_L
17	Rolandic_Oper_L	46	Cuneus_R	75	Pallidum_L	104	Cerebelum_8_R
18	Rolandic_Oper_R	47	Lingual_L	76	Pallidum_R	105	Cerebelum_9_L
19	Supp_Motor__L	48	Lingual_R	77	Thalamus_L	106	Cerebelum_9_R
20	Supp_Motor__R	**49**	**Occipital_Sup_L**	78	Thalamus_R	107	Cerebelum_10_L
21	Olfactory_L	**50**	**Occipital_Sup_R**	79	Heschl_L	108	Cerebelum_10_R
22	Olfactory_R	**51**	**Occipital_Mid_L**	80	Heschl_R	109	Vermis_1_2
23	Frontl_Sup_Medl_L	**52**	**Occipital_Mid_R**	**81**	**Temporal_Sup_L**	110	Vermis_3
24	Frontl_Sup_Med_R	**53**	**Occipital_Inf_L**	**82**	**Temporal_Sup_R**	111	Vermis_4_5
25	Frontal_Mid_Orb_L	**54**	**Occipital_Inf_R**	**83**	**Templ_Pole_Sup_L**	112	Vermis_6
26	Frontal_Mid_Orb_R	**55**	**Fusiform_L**	**84**	**Templ_Pole_Sup_R**	113	Vermis_7
27	Rectus_L	**56**	**Fusiform_R**	**85**	**Temporal_Mid_L**	114	Vermis_8
28	Rectus_R	**57**	Postcentral_L	**86**	**Temporal_Mid_R**	115	Vermis_9
29	Insula_L	58	Postcentral_R	**87**	**Templ_Pole_Mid_L**	116	Vermis_10

3. SPARSE INVERSE COVARIANCE ESTIMATION

In this section, we briefly introduce the sparse inverse covariance estimation as well as some related work with the emphasis on numerical algorithms.

Suppose we have n samples independently drawn from a multivariate Gaussian distribution, and these samples are denoted as $x_1, \cdots, x_n \sim \mathcal{N}(\mu, \Sigma)$, where x_i is a p-dimension vector, $\mu \in I\!R^p$ is the mean, and $\Sigma \in I\!R^{p\times p}$ is the covariance to be estimated. Let $\Theta = \Sigma^{-1}$ be the inverse covariance (or precision) matrix. The empirical covariance is denoted as S:

$$S = \frac{1}{n}\sum_{i=1}^{n}(x_i - \mu)(x_i - \mu)^T.$$

It is straightforward to derive that the maximum log likelihood of inverse covariance matrix under a multivariate Gaussian model. Formally, the maximum likelihood estimate of $\Theta = \Sigma^{-1}$ can be obtained by maximizing

$$\max_{\Theta \succ 0} f = \log\det\Theta - \mathrm{tr}\left(S\Theta\right), \tag{1}$$

where $\mathrm{tr}\left(S\Theta\right)$ is the trace of $S\Theta$. Assume that S is nonsingular. Computing the derivative of f w.r.t. Θ and setting it to zero, we get

$$\Theta^{-1} - S = 0.$$

Thus, the maximum likelihood estimate of the inverse covariance Θ is $\Theta = S^{-1}$. If the dimensionality is larger than the sample size, i.e., $p > n$, some types of regularization are necessary in order to estimate Θ since S is singular. The connection between the estimation of Θ and S in Eq. (1) suggests the possibility that we can obtain shrunken estimates through maximization of the penalized log likelihood function. Formally, we estimate $\Theta = \Sigma^{-1}$ by maximizing

the following objective function:

$$\log\det\Theta - \mathrm{tr}\,(S\Theta) - \lambda J(\Theta), \tag{2}$$

where $J(\Theta)$ is a penalty function. In particular, in this paper we consider the following formulation of $J(\Theta)$:

$$J(\Theta) = \|\mathrm{vec}(\Theta)\|_1, \tag{3}$$

where $\mathrm{vec}(\Theta)$ is the vector form of matrix Θ. In other words, $\|\mathrm{vec}(\Theta)\|_1$ denotes the sum of the absolute values of all elements of the positive definite matrix Θ.

It is well-known that model sparsity can often be achieved by applying the ℓ_1-norm regularization [10, 26]. This has been introduced into the least squares formulation and the resulting model is called lasso [26]. Similarly, the formulation in Eq. (2) with $J(\Theta)$ defined in Eq. (3) produces a sparse estimate for Θ. Specifically, if the ijth component of the inverse covariance matrix Θ is zero, then variables i and j are conditionally independent, given the other variables in the multivariate Gaussian distribution. Thus, it makes sense to impose the ℓ_1 penalty to the estimation of Θ to increase its sparsity as in lasso [26].

3.1 Related Work

A number of papers in the literature are devoted to the estimation of covariance matrices. It is observed that the covariance matrix can be estimated robustly when enough entries of the inverse covariance matrix are set to zero [8]. Meanwhile, it has been demonstrated in the literature that many biomedical and genetic networks are not fully connected and many genetic interaction networks contain many genes with few interactions and a few genes with many interactions [25, 13]. Therefore, many biomedical and genetic networks are intrinsically sparse and the corresponding inverse covariance matrix is sparse. These observations in theory and practice motivate the development of efficient and effective sparse inverse covariance estimates.

In Gaussian graphical model [16], it assumes that the multivariate vector follows a multivariate normal distribution with a particular structure of the inverse covariance structure, a.k.a. precision or concentration matrix. It usually assumes that the patterns of some variables can be predicted by a small subset of all variables. This assumption leads to sparsity in the precision matrix of the multivariate distribution, and results in the so-called neighborhood selection or covariance selection problem [8]. In other words, zeros in the inverse covariance matrix correspond to conditional independence properties among the variables. In this setting, a sparse inverse covariance matrix, if it fits the data well, is very useful to practitioners, as it simplifies the understanding, and provides the insights into the data.

To determine the zero patterns in the inverse covariance matrix, the traditional method is based on the greedy forward-backward search algorithm [16]. Recently, some algorithms are proposed to solve sparse inverse covariance matrix. A gradient descent algorithm is proposed in [17] in which the sparse inverse covariance is computed by defining a loss function that is the negative of the log likelihood function. A penalized maximum likelihood estimation is considered in [15]. In [6], a set of large-scale methods are proposed to solve problems where a sparse structure of inverse covariance is known a prior. The interior point method for the "maxdet" problem is proposed [18]. In [2], the ℓ_1-norm regularization is considered, and two efficient algorithms are proposed: one is based on Nesterov's first-order algorithm [22] which yields a rigorous complexity estimate; the second one uses the block coordinate decent approach to update rows/columns of the covariance matrix sequentially. The block coordinate decent algorithm is further improved in [12].

4. THE PROPOSED ALGORITHM

In this section, we present the proposed algorithm for solving the following optimization problem:

$$\max_{\Theta\succ 0} \quad \log\det\Theta - \mathrm{tr}(S\Theta) - \lambda\|\mathrm{vec}(\Theta)\|_1, \tag{4}$$

where S is the empirical covariance matrix, and λ is the regularization parameter.

One drawback of many existing algorithms [12, 2] is that they directly estimate the covariance matrix. Since the goal is to estimate the sparsity structure of the inverse covariance matrix, a better approach is to compute the inverse covariance matrix directly. This also facilitates the incorporation of the user feedback (e.g., prior domain knowledge) into the formulation. The proposed approach estimates the inverse covariance matrix Θ directly, and it also follows the framework of the block coordinate descent [12, 2]. Specifically, we partition S and Θ in the form of block matrix:

$$S = \begin{bmatrix} S_{11} & s_{12} \\ s_{12}^T & s_{22} \end{bmatrix}, \Theta = \begin{bmatrix} \Theta_{11} & \theta_{12} \\ \theta_{12}^T & \theta_{22} \end{bmatrix},$$

where $S_{11}, \Theta_{11} \in I\!R^{(p-1)\times(p-1)}$, $s_{12}, \theta_{12} \in I\!R^{p-1}$, and $s_{22}, \theta_{22} \in I\!R$. Then we can reformulate $\log\det\Theta$ as follows:

$$\begin{aligned} \log\det\Theta &= \log\left(\det\Theta_{11}(\theta_{22} - \theta_{12}^T\Theta_{11}^{-1}\theta_{12})\right) \\ &= \log\det\Theta_{11} + \log\left(\theta_{22} - \theta_{12}^T\Theta_{11}^{-1}\theta_{12}\right). \end{aligned}$$

Thus, the problem in Eq. (4) can be formulated as:

$$\begin{aligned} \max_{\Theta\succ 0} f \;=\; & \log\det\Theta_{11} + \log\left(\theta_{22} - \theta_{12}^T\Theta_{11}^{-1}\theta_{12}\right) \\ & -\mathrm{tr}(S\Theta) - \lambda\|\mathrm{vec}(\Theta))\|_1. \end{aligned} \tag{5}$$

In the block coordinate descent approach, we update each row/column while fixing other elements of matrix Θ in each iteration. To compute the optimal Θ, we use $(S+\lambda I)^{-1}$ as the initial guess of Θ, then update each row/column of Θ repeatedly until convergence.

In the following, we assume that Θ_{11} is fixed and we need to update θ_{12} and θ_{22}. We can apply similar techniques to update other rows/columns. The subdifferential of f w.r.t. θ_{12} can be computed as follows:

$$\partial f = -\frac{2}{\theta_{22} - \theta_{12}^T\Theta_{11}^{-1}\theta_{12}}\Theta_{11}^{-1}\theta_{12} - 2s_{12} - 2\lambda\mathrm{SGN}(\theta_{12}), \tag{6}$$

where $\mathrm{SGN}(t)$ is a set-valued mapping for $t \in I\!R$, and it is defined as:

$$\mathrm{SGN}(t) := \begin{cases} \{1\} & t > 0, \\ [-1,1] & t = 0, \\ \{-1\} & t < 0. \end{cases} \tag{7}$$

In fact, $\mathrm{SGN}(t)$ is the subdifferential of $|t|$. For the vector $v \in I\!R^p$, $\mathrm{SGN}(v)$ is defined component-wise, i.e., the ith component of $\mathrm{SGN}(v)$ is defined as $\mathrm{SGN}(v_i)$ where v_i is the ith component of v. Clearly, $\mathrm{SGN}(v)$ is the subdifferential of $\|v\|_1$.

We also compute the subgradient of f with respect to θ_{22}. Note that $\theta_{22} > 0$. We have

$$\begin{aligned} \partial f &= \frac{1}{\theta_{22} - \theta_{12}^T \Theta_{11}^{-1} \theta_{12}} - s_{22} - \lambda = 0 \\ \Leftrightarrow \quad & \theta_{22} - \theta_{12}^T \Theta_{11}^{-1} \theta_{12} = \frac{1}{s_{22} + \lambda} > 0. \end{aligned} \tag{8}$$

The inequality in Eq. (8) guarantees the positive definiteness of Θ. Let

$$\alpha = -\frac{\theta_{12}}{\theta_{22} - \theta_{12}^T \Theta_{11}^{-1} \theta_{12}} = -(s_{22} + \lambda)\theta_{12}.$$

It is clear that $\mathrm{SGN}(\alpha) = -\mathrm{SGN}(\theta_{12})$. Then we can represent the subdifferential of Eq. (6) as:

$$\partial f = 2\Theta_{11}^{-1}\alpha - 2s_{12} + 2\lambda \mathrm{SGN}(\alpha).$$

It is clear that ∂f is (a constant multiple of) the subdifferential of the following optimization problem:

$$\min_{\alpha} g = \frac{1}{2}\alpha^T \Theta_{11}^{-1} \alpha - s_{12}^T \alpha + \lambda \|\alpha\|_1. \tag{9}$$

Thus, the problem in Eq. (4) is equivalent to the one in Eq. (9) if Θ_{11} is fixed. Note that the problem in Eq. (9) is equivalent to the following min-max problem:

$$\max_{\kappa} \min_{\alpha} h(\alpha, \kappa) = \left(-\frac{1}{2}\kappa^T \Theta_{11} \kappa + \kappa^T \alpha \right) - s_{12}^T \alpha + \lambda \|\alpha\|_1. \tag{10}$$

The equivalence relationship can be verified easily by computing the derivative of $h(\alpha, \kappa)$ w.r.t. κ:

$$-\Theta_{11}\kappa + \alpha = 0 \Leftrightarrow \kappa = \Theta_{11}^{-1}\alpha. \tag{11}$$

Thus, κ can be eliminated and the resulting problem is equivalent to Eq. (9). In practice, we use the prox method [21] to solve the min-max problem.

When α is solved, we can recover $\theta_{12} = -\frac{1}{s_{22}+\lambda}\alpha$. Next we show how to derive θ_{22}. From Eq. (8), we have

$$\begin{aligned} \theta_{22} &= \theta_{12}^T \Theta_{11}^{-1} \theta_{12} + \frac{1}{s_{22} + \lambda} \\ &= \theta_{12}^T \Theta_{11}^{-1} \left(-\frac{\alpha}{s_{22} + \lambda} \right) + \frac{1}{s_{22} + \lambda} \\ &= -\frac{1}{s_{22} + \lambda} \theta_{12}^T \kappa + \frac{1}{s_{22} + \lambda} \\ &= \frac{1}{s_{22} + \lambda} \left(-\theta_{12}^T \kappa + 1 \right). \end{aligned}$$

The outline of the proposed algorithm is given in Algorithm 1. The global convergence of Algorithm 1 is guaranteed due to the separability of the non-smooth ℓ_1 penalty term [27]. We have following property:

THEOREM 1. *The produced $\Theta^{(j)}$ at the j-th iteration is strictly positive definite, i.e., for $1 \leq j \leq p, \Theta^{(j)} \succ 0$. Furthermore, the updating of θ_{12} and θ_{22} at each iteration permits a unique solution.*

PROOF. Note that if Θ_{11} is positive definite, the problem in Eq. (9) is strictly convex, then the unique solution of α is guaranteed. Hence, we can obtain unique solutions of θ_{12} and θ_{22}. Therefore, it suffices to show that $\Theta^{(i)}$ is positive definite at each step in Algorithm 1.

We use mathematical induction to prove the positive definiteness of $\Theta^{(i)}, 1 \leq i \leq p$. Note that $\Theta^{(0)} \succ 0$, thus the proposition is true in the basis step. Next suppose that $\Theta^{(i)} \succ 0$, we consider $\Theta^{(i+1)}$ after one iteration. It follows from Eq. (8) that at each step we have

$$\theta_{22} - \theta_{12}^T \Theta_{11}^{-1} \theta_{12} = \frac{1}{s_{22} + \lambda} > 0$$

Thus, we have

$$\det \Theta^{(i+1)} = \det \Theta_{11}^{(i)} \left(\theta_{22}^{(i+1)} - {\theta_{12}^{(i+1)}}^T {\Theta_{11}^{(i)}}^{-1} \theta_{12}^{(i+1)} \right) > 0.$$

Note that $\Theta_{11}^{(i)}$ is positive definite since $\Theta^{(i)} \succ 0$, thus $\Theta^{(i+1)}$ is also positive definite after this iteration. □

Algorithm 1 Sparse Inverse Covariance Estimation

Input: empirical covariance S, parameter λ
Initialize $\Theta^{(0)} := (S + \lambda I)^{-1}$
repeat
  for $j = 1$ **to** p **do**
    Let $\Theta^{(j-1)}$ denote the current iterate. Solve the min-max problem:

$$\max_{\kappa} \min_{\alpha} h(\alpha, \kappa) = \left(-\frac{1}{2}\kappa^T \Theta_{11} \kappa + \kappa^T \alpha \right) - s_{12}^T \alpha + \lambda \|\alpha\|_1.$$

    Compute $\hat{y}$:

$$\hat{y} = -\frac{\alpha}{s_{22} + \lambda}.$$

    Compute $\hat{\theta}_{jj}$:

$$\hat{\theta}_{jj} = \frac{1}{s_{22} + \lambda} \left(-\theta_{12}^T \kappa + 1 \right)$$

    Update rule: $\Theta^{(j)}$ is $\Theta^{(j-1)}$ with column/row replaced by $[\hat{y}; \hat{\theta}_{jj}]$.
  end for
until converge

We check the convergence of Algorithm 1 by comparing the Θ matrices between two consecutive iterations. More specifically, let Θ^{new} and Θ^{old} be the solutions at the current and previous iterations, respectively. Then, the algorithm stops if $||\Theta^{new} - \Theta^{old}||_F \leqslant \epsilon$ holds for a certain threshold ϵ. We set $\epsilon = 10^{-4}$ in our experiments.

Compared with the algorithms discussed in the last section, the proposed Algorithm 1 directly estimates the inverse covariance matrix Θ. Thus, it facilitates the incorporation of the user feedback (e.g., prior domain knowledge) by imposing constraints to guide the optimization problem. For example, we can set $\theta_{ij} = 0$ if the ith region and the jth region are known to be disconnected. Note that $\alpha = -(s_{22} + \lambda)\theta_{12}$ in each iteration of the block coordinate descent approach, thus $\theta_{ij} = 0$ implies that the corresponding entry in α is 0. Hence, we can enforce the corresponding entries in α to be 0 in each iteration. For a given Θ_{11}, the optimization problem in Eq. (9) can be reformulated as follows:

$$\begin{aligned} \min_{\alpha} \quad & g = \alpha^T \Theta_{11}^{-1} \alpha - s_{12}^T \alpha + \lambda \|\alpha\|_1 && (12) \\ \text{s.t.} \quad & \alpha_i = 0 \quad \text{if } i \in V, && (13) \end{aligned}$$

where V is the set of indices (based on the user feedback) corresponding to zero entries in α. Note that this problem is also strictly convex and can be solved efficiently. Similarly, we can recover θ_{12} and θ_{22} from α.

5. EXPERIMENTS

We have performed experiments on the PET-AAL data which is acquired and preprocessed using the methods discussed in Section 2. We applied the proposed algorithm to three different groups, including Normal Control (NC), Mild Cognition Impairment (MCI) and Alzheimer's Disease (AD) patients. We set $\lambda = 1.1$ in all experiments. The regions considered in this study are the ones marked in bold type in Table 2. These regions are identified as being significantly impacted by AD. The names of regions with "L" stand for regions in the left hemisphere of the brain, and those with "R" stand for regions in the right hemisphere.

The resulting connectivity among different brain regions for AD, MCI, and NC are shown in Figures 1, 2, and 3, respectively. The resulting sparse inverse covariance matrix is represented using a graph, where nodes correspond to the regions of the brain, and the edges connecting the nodes define the conditional partial correlation between the nodes. Specifically, if $\Theta(i, j) = 0$, then regions i and j are conditionally independent, and there is no edge between them.

From these figures, we observe several interesting patterns in the brain network for each of the 3 diagnostic groups. Comparing Figures 1, 2, and 3, we can observe that the Occipital regions and the Temporal regions in MCI's are not as strongly connected as in NC's. As for the AD patients, we can observe from Figure 1 that these two types of regions are completely set apart. It can also be observed that hippocampus and parahippocampal gyrus interact with other regions in NC's, while they become isolated in AD's and MCI's. The connectivity among the these four regions including Hippocampus_L, Hippocampus_R, ParaHippocampal_L, and ParaHippocampal_R also becomes weaker in AD's and MCI's. The hippocampus belongs to the limbic system and plays major roles in short-term memory and spatial navigation. In AD, the hippocampus is one of the first regions of the brain to suffer damage, which results in memory problems among the first symptoms. Our experimental results clearly demonstrate that AD patients show a decreased level of functional connectivity within this network, which is consistent of the findings in AD study [29].

We can observe from Figure 2 that the edge between Occipital_Mid_R and Temporal_Mid_R is the only connection between the Occipital and Temporal regions, while these two regions are completely separated in AD as shown in Figure 1. To test the significance of the connectivity between these two types of regions, we run the algorithm under the constraint that Occipital_Mid_R and Temporal_Mid_R are isolated. The results are summarized in Figure 4. It is shown that the Occipital and Temporal regions are still connected with a link between Occipital_Inf_R and Temporal_Mid_R.

Next, we investigate the robustness of the generated network in AD study. Recall that one key feature of the proposed SICE algorithm is that it allows the user feedback to be incorporated into the estimation process by imposing additional constraints in the optimization formulation. In this experiment we study how the connectivity changes as more constraints are enforced in the network. Since the patterns in AD patients are of great interest, we focus on the AD subjects. Specifically, we remove five links in the network in Figure 1: the link between Temporal_Pole_Mid_R and Temporal_Pole_Inf_R_8302, the link between Cingulum_Post_L and Cingulum_Post_R, the link between Hippocampus_L and Par -raHippocampal_L, the link between Temporal_Sup_R and Temporal_Mid_R, the link between Temporal_Pole_Mid_L and Temporal_Pole_Sup_R. We then run the algorithm under the above constraints. The results are summarized in Figure 5. It can be observed that the connectivity in the subgraph including the occipital and parietal regions remains almost the same. The experimental results show that the perturbation tends to affect the local topology of the generated network only. We performed several other similar studies and observed a similar trend.

We compute the empirical correlation between twelve occipital and parietal regions (form a subgraph) of AD patients. The results are summarized in Table 3. The entries corresponding to the connections in the network generated by the proposed algorithm are highlighted in bold type and red color. We can observe from the table that a large correlation usually implies connectivity in the graph. However, it is not always the case, e.g., the $(2, 6)$th entry. This may be due to the fact that the correlation captures the pairwise information only, while the sparse inverse covariance estimation captures the interaction among all regions.

6. CONCLUSIONS AND FUTURE WORK

In this paper, we propose a novel sparse inverse covariance estimation algorithm to discover the connectivity among different brain regions for AD study. One appealing feature of the proposed algorithm is that it can incorporate the user feedback into the estimation process, while the connectivity patterns can be discovered automatically. Our experimental results on a collection of FDG-PET images demonstrate the effectiveness of the proposed algorithm for analyzing brain region connectivity for Alzheimer's disease study.

We plan to develop an interactive software tool to help AD domain experts to investigate the connectivity among different brain regions. The typical diagnosis is an interactive process, in which the prior knowledge can be obtained and updated. We aim to integrate such prior knowledge seamlessly and reveal the connectivity more precisely.

Functional magnetic resonance imaging (fMRI) is a procedure that is widely used for human brain function analysis in normal controls as well as in diseased individuals. Most recently, it has been used to study the intrinsic activity and connectivity of the brain under resting condition (i.e., there is no cognitive task), a.k.a the default mode network (DMN). Recent researches have found significantly different DMN differences between AD patients and NC, opening the possibility of using the resting DMN as an AD diagnosis biomarker. We plan to investigate the functional MRI data for Alzheimer's disease study using the proposed algorithm.

Acknowledgments

This research is sponsored in part by the Arizona Alzheimer's Consortium and by NSF IIS-0612069 and IIS-0812551.

Data collection and sharing for this research was funded by the Alzheimer's Disease Neuroimaging Initiative (ADNI; PI: Michael Weiner; NIH grant U01 AG024904). ADNI is funded by the National Institute on Aging, the National Institute of Biomedical Imaging and Bioengineering (NIBIB), and through generous contributions from the following: Pfizer Inc., Wyeth Research, Bristol-Myers Squibb, Eli Lilly and Company, GlaxoSmithKline, Merck & Co. Inc., AstraZeneca AB, Novartis Pharmaceuticals Corporation, Alzheimer's Association, Eisai Global Clinical Development, Elan Corpora-

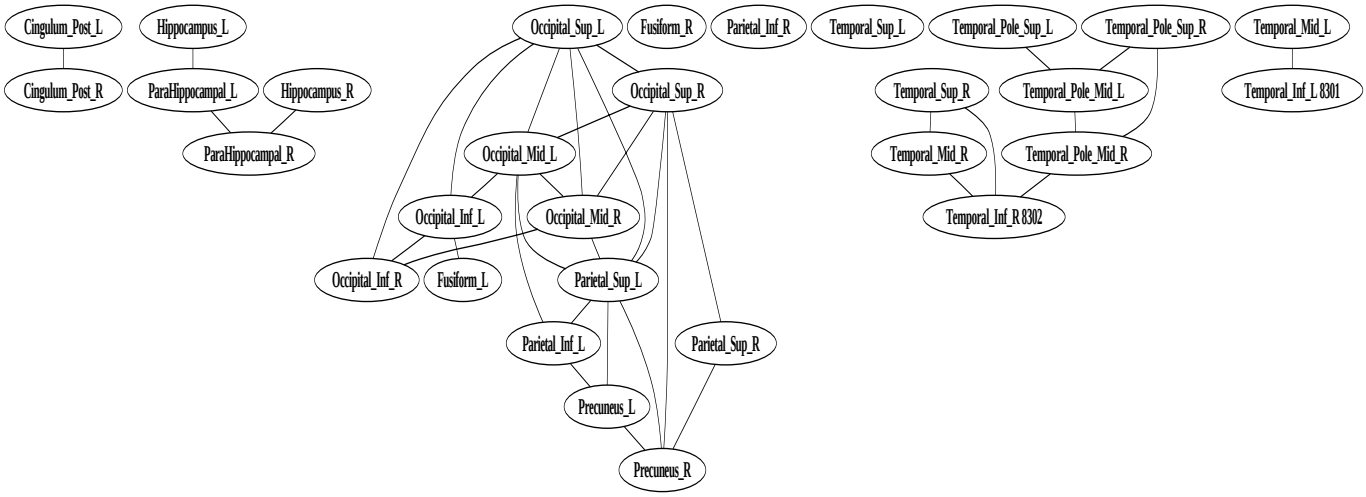

Figure 1: The connectivity among different brain regions for AD patients.

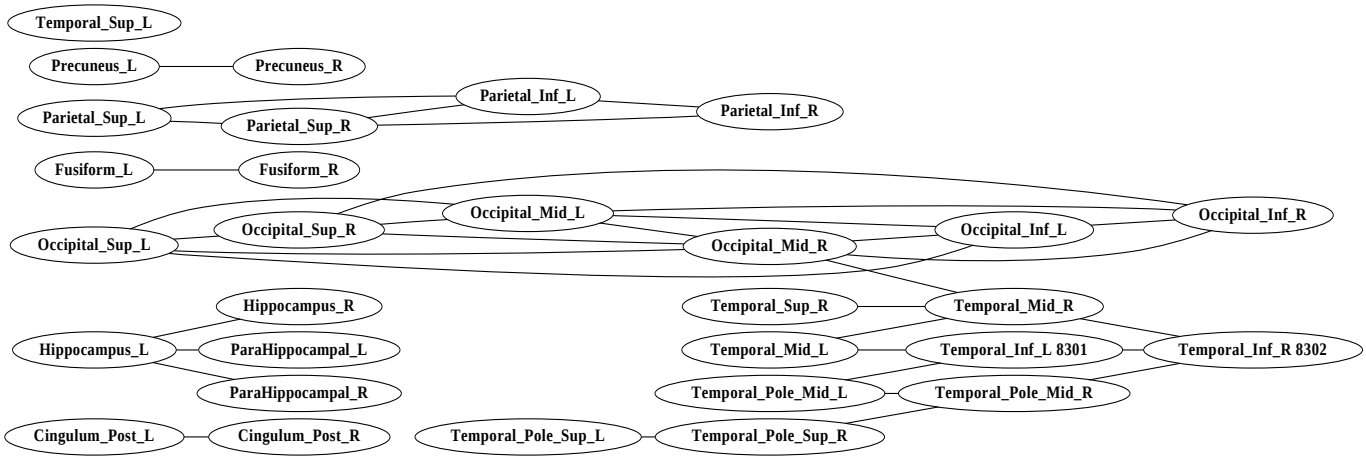

Figure 2: The connectivity among different brain regions for Mild Cognition Impairment patients.

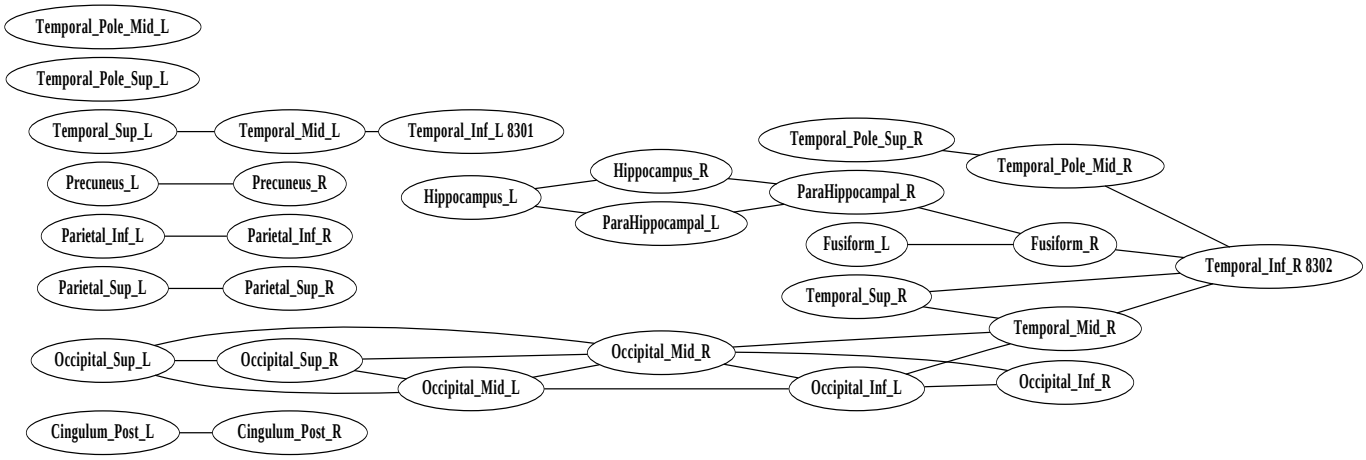

Figure 3: The connectivity among different brain regions for Normal Controls.

Table 3: The empirical correlation matrix of the 12 brain regions for AD patients. Each row/column in the table corresponds to a region. The (i, j)th entry is the correlation between the ith region and the jth region. The entries highlighted in bold type and red color correspond to a connection in the network generated by the proposed algorithm. These 12 regions include: Occipital_Sup_L, Occipital_Sup_R, Occipital_Mid_L, Occipital_Mid_R, Occipital_Inf_L, Occipital_Inf_R, Fusiform_L, Parietal_Sup_L, Parietal_Sup_R, Parietal_Inf_L Precuneus_L, and Precuneus_R.

1.00	**0.83**	**0.91**	**0.75**	**0.79**	0.66	0.50	**0.78**	0.48	0.63	0.67	0.54
0.83	**1.00**	**0.71**	**0.90**	0.57	0.76	0.20	**0.78**	**0.71**	0.54	0.60	**0.71**
0.91	**0.71**	**1.00**	**0.72**	**0.92**	0.62	0.67	**0.73**	0.40	**0.68**	0.64	0.44
0.75	**0.90**	**0.72**	**1.00**	0.64	**0.86**	0.29	**0.68**	0.61	0.48	0.44	0.56
0.79	0.57	**0.92**	0.64	**1.00**	**0.65**	**0.77**	0.57	0.25	0.50	0.44	0.26
0.66	0.76	0.62	**0.86**	**0.65**	**1.00**	0.32	0.55	0.48	0.33	0.31	0.41
0.50	0.20	0.67	0.29	**0.77**	0.32	**1.00**	0.28	-0.02	0.20	0.26	0.01
0.78	**0.78**	**0.73**	**0.68**	0.57	0.55	0.28	**1.00**	0.81	**0.81**	**0.82**	**0.71**
0.48	**0.71**	0.40	0.61	0.25	0.48	-0.02	0.81	**1.00**	0.54	0.55	**0.66**
0.63	0.54	**0.68**	0.48	0.50	0.33	0.20	**0.81**	0.54	**1.00**	**0.83**	0.66
0.67	0.60	0.64	0.44	0.44	0.31	0.26	**0.82**	0.55	**0.83**	**1.00**	**0.80**
0.54	**0.71**	0.44	0.56	0.26	0.41	0.01	**0.71**	**0.66**	0.66	**0.80**	**1.00**

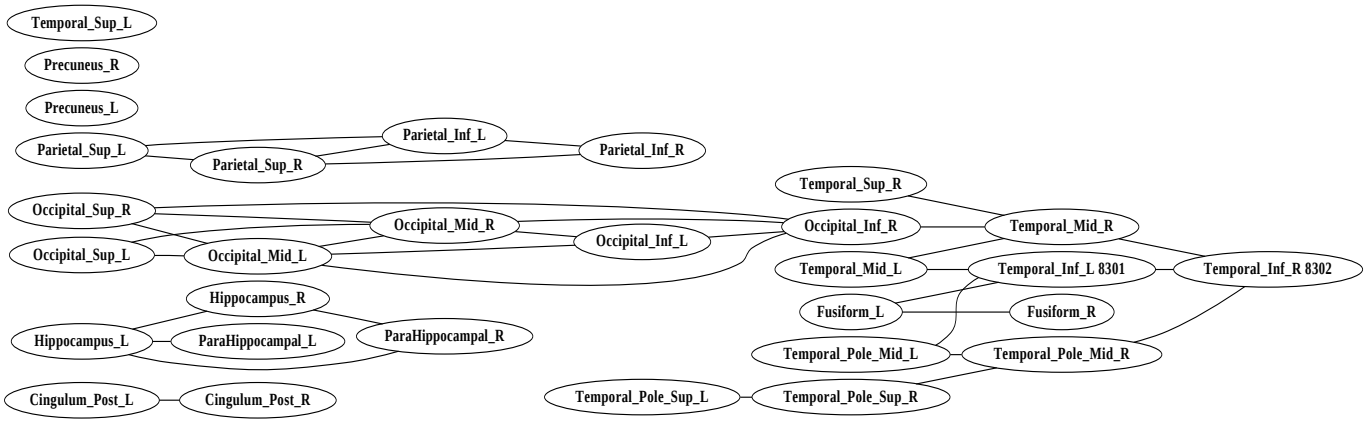

Figure 4: The connectivity among different brain regions for Mild Cognition Impairment patients after removing one link between Occipital_Mid_R and Temporal_Mid_R.

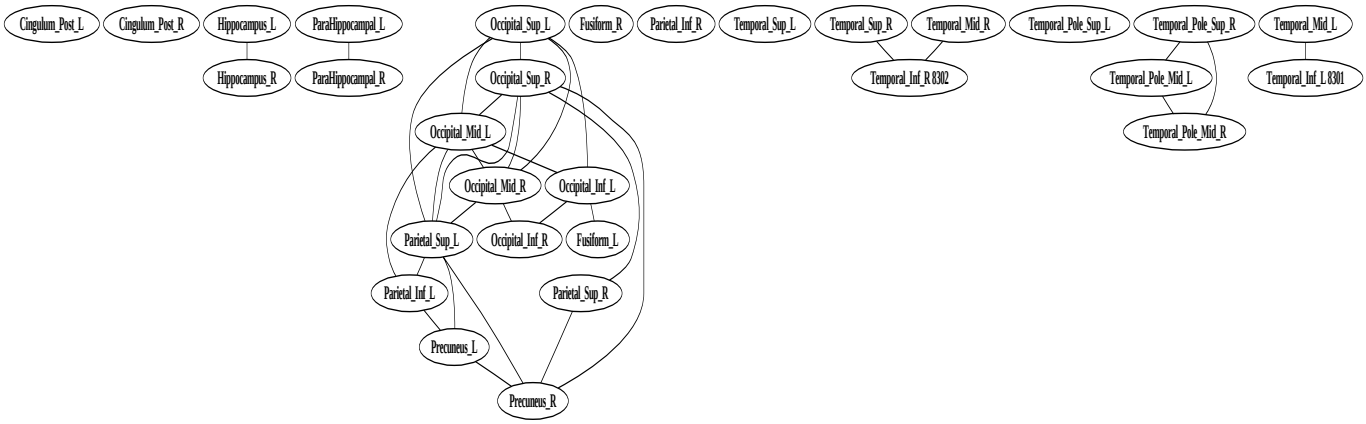

Figure 5: The connectivity among different brain regions for AD patients after removing five links (see the texts for details).

tion plc, Forest Laboratories, and the Institute for the Study of Aging, with participation from the U.S. Food and Drug Administration. Industry partnerships are coordinated through the Foundation for the National Institutes of Health. The grantee organization is the Northern California Institute for Research and Education, and the study is coordinated by the Alzheimer's Disease Cooperative Study at the University of California, San Diego. ADNI data are disseminated by the Laboratory of NeuroImaging at the University of California, Los Angeles.

7. REFERENCES

[1] G. Alexander and E. Reiman. Neuroimaging. In M.F. Weiner and A.M. Lipton, editors, *The dementias: diagnosis, treatment and research*, 2003.

[2] O. Banerjee, L. El Ghaoui, and A. d'Aspremont. Model selection through sparse maximum likelihood estimation for multivariate Gaussian or binary data. *Journal of Machine Learning Ressearch*, 9:485–516, 2008.

[3] O. Banerjee, L. El Ghaoui, A. d'Aspremont, and G. Natsoulis. Convex optimization techniques for fitting sparse Gaussian graphical models. In *ICML*, pages 89–96, 2006.

[4] A. Berge, A.C. Jensen, and A.H.S. Solberg. Sparse inverse covariance estimates for hyperspectral image classification. *Geoscience and Remote Sensing, IEEE Transactions on*, 45(5):1399–1407, 2007.

[5] J.A. Bilmes. Factored sparse inverse covariance matrices. In *ICASSP*, pages 1009–1012, 2000.

[6] J. Dahl, L. Vandenberghe, and V. Roychowdhury. Covariance selection for nonchordal graphs via chordal embedding. *Optimization Methods Software*, 23(4):501–520, 2008.

[7] X. Delbeuck, M. Van der Linden, and F. Collette. Alzheimer's disease as a disconnection syndrome? *Neuropsychology Review*, 13(2):79–92, 2003.

[8] A.P. Dempster. Covariance selection. *Biometrics*, 28(1):157–175, 1972.

[9] A. Dobra, C. Hans, B. Jones, J. R. Nevins, G. Yao, and M. West. Sparse graphical models for exploring gene expression data. *Journal of Multivariate Analysis*, 90(1):196–212, 2004.

[10] D.L. Donoho. For most large underdetermined systems of linear equations, the minimal 11-norm near-solution approximates the sparsest near-solution. *Communications on Pure and Applied Mathematics*, 59(7):907–934, 2006.

[11] M.F. Folstein, S. Folstein, and P.R. McHugh. Minimental state: a practical method for grading the cognitive state of patients for the clinician. *Journal of Psychiatric Research*, 12(3):189–198, 1975.

[12] J. Friedman, T. Hastie, and R. Tibshirani. Sparse inverse covariance estimation with the graphical lasso. *Biostatistics*, 8(1):1–10, 2007.

[13] T.S. Gardner, D. di Bernardo, D. Lorenz, and J.J. Collins. Inferring genetic networks and identifying compound mode of action via expression profiling. *Science*, 301(5629):102–105, 2003.

[14] L. Heston and J. White. *The vanishing mind: A practical guide to Alzheimer's disease and other dementias*. W. H. Freeman and Co., New York, 1983.

[15] J.Z. Huang, N. Liu, M. Pourahmadi, and L. Liu. Covariance matrix selection and estimation via penalised normal likelihood. *Biometrika*, 93(1):85–98, 2006.

[16] S.L. Lauritzen. *Graphical models*. Oxford University Press, Clarendon, 1996.

[17] H. Li and J. Gui. Gradient directed regularization for sparse Gaussian concentration graphs, with applications to inference of genetic networks. *Biostatistics*, 7(2):302–317, 2005.

[18] Y. Lin. Model selection and estimation in the Gaussian graphical model. *Biometrika*, 94(1):19–35, 2007.

[19] G. McKhann, D. Drachman, and M. Folstein. Mental and clinical diagnosis of alzheimer's disease: report of the nincdsadrda work group under the auspices of the department of health and human services task force on alzheimers disease. *Neurology*, 34(7):939–944, 1984.

[20] S. Molchan. The Alzheimer's disease neuroimaging initiative. *Business Briefing: US Neurology Review*, pages 30–32, 2005.

[21] A. Nemirovski. Prox-method with rate of convergence $o(1/t)$ for variational inequalities with lipschitz continuous monotone operators and smooth convex-concave saddle point problems. *SIAM Journal on Optimization*, 15(1):229–251, 2005.

[22] Y. Nesterov. Smooth minimization of non-smooth functions. *Mathematical Programming*, 103(1):127–152, 2005.

[23] C.J. Stam, B.F. Jones, G. Nolte, M. Breakspear, and P. Scheltens. Small-world networks and functional connectivity in Alzheimer's disease. *Cereb Cortex*, 17:92–99, 2007.

[24] K. Supekar, V. Menon, D. Rubin, M. Musen, and M.D. Greicius. Network analysis of intrinsic functional brain connectivity in alzheimer's disease. *PLoS Computational Biology*, 4(6):e1000100, 2008.

[25] J. Tegner, M.K. Yeung, J. Hasty, and J.J. Collins. Reverse engineering gene networks: integrating genetic perturbations with dynamical modeling. *Proceedings of the National Academy of Sciences*, 100(10):5944–5949, 2003.

[26] R. Tibshirani. Regression shrinkage and selection via the lasso. *Journal of the Royal Statistical Society Series B*, 58(1):267–288, 1996.

[27] P. Tseng. Convergence of block coordinate descent method for nondifferentiable maximation. *J. Opt. Theory and Applications*, 109(3):474–494, 2001.

[28] N. Tzourio-Mazoyer, B. Landeau, D. Papathanassiou, F. Crivello, O. Etard, N. Delcroix, B. Mazoyer, and M. Joliot. Automated anatomical labeling of activations in spm using a macroscopic anatomical parcellation of the mni mri single-subject brain. *NeuroImage*, 15(1):273–289, 2002.

[29] S. Wakana, H. Jiang, L.M. Nagae-Poetscher, P.C. van Zijl, and S. Mori. Fiber tract-based atlas of human white matter anatomy. *Radiology*, 230(1):77–87, 2004.

[30] J. Ye, K. Chen, T. Wu, J. Li, Z. Zhao, R. Patel, M. Bae, R. Janardan, H. Liu, G. Alexander, and E. Reiman. Heterogeneous data fusion for Alzheimer's disease study. In *KDD*, pages 1025–1033, 2008.